

# The Temperature–Humidity Covariance in the Marine Surface Layer: A One-dimensional Analytical Model

Gabriel G. Katul · Anna M. Sempreviva ·  
Daniela Cava

Received: 25 May 2007 / Accepted: 4 October 2007 / Published online: 26 October 2007  
© Springer Science+Business Media B.V. 2007

**Abstract** An analytical model that predicts how much of the temperature–humidity covariance within the marine atmospheric surface layer (ASL) originates just above the ASL and just near the surface is proposed and tested using observations from the *Risø Air Sea Experiment* (RASEX). The model is based on a simplified budget for the two-scalar covariance that retains three basic terms: production, dissipation, and vertical transport. Standard second-order closure formulations are employed for the triple moments and the dissipation terms, and the canonical mixing length for the closure model is assumed linear with height ( $z$ ) from the surface. Despite the poor performance of the gradient–diffusion closure in reproducing the measured triple moment, the overall covariance model was shown to be sufficiently robust to these assumptions. One of the main findings from the analytical treatment is the origin of the asymmetry in how the top and bottom boundary conditions affect the two-scalar covariance in the ASL. The analytical model reveals that ‘bottom-up’ boundary-condition variations scale with  $z^{-\sqrt{a}}$ , while ‘top-down’ variations scale with  $z^{\sqrt{a}}$ , where  $a$  is a constant that can be derived from similarity and closure constants. The genesis of this asymmetry

---

G. G. Katul (✉)

Nicholas School of the Environment and Earth Sciences, Duke University, Box 90328, Durham, NC, 27708-0328, USA  
e-mail: gaby@duke.edu

G. G. Katul

Department of Civil and Environmental Engineering, Duke University, Durham, NC, 27708-0328, USA

A. M. Sempreviva

Department of Wind Energy, Risø National Laboratory, Technical University of Denmark, 4000 Roskilde, Denmark  
e-mail: Anna.sempreviva@risoe.dk

A. M. Sempreviva

Institute of Atmospheric Sciences and Climate, ISAC-CNR, Area di Ricerca CNR, Roma Tor Vergata, Via Fosso del Cavaliere 10, 00133 Rome, Italy  
e-mail: am.sempreviva@isac.cnr.it

D. Cava

CNR – Institute of Atmosphere Sciences and Climate Section of Lecce, Lecce, Italy  
e-mail: d.cava@isac.cnr.it

stems from the flux-transport term but is modulated by the dissipation, and persists even in the absence of any inhomogeneity in the local production function. It is shown that the local production function acts to adjust the relative proportions of these two boundary conditions with weights that vary with the Obukhov length. The findings here do not provide ‘finality’ to the discussions on the covariance between humidity and temperature or the role of entrainment in modulating the turbulence within the ASL. Rather, they are intended to guide new hypotheses about interpretations of existing field data and identify needs for future field and numerical experiments.

**Keywords** Atmospheric surface layer · Cauchy–Euler equation · Gradient–diffusion closure · Marine surface layer · Risø Air Sea experiment · Temperature–humidity covariance

## 1 Introduction

Over the last three decades, the temperature ( $T$ )–humidity ( $C$ ) covariance ( $\overline{T'C'}$ ) in the atmospheric surface layer (ASL) has received significant attention, partly because of its use in assessing similarities in bulk scalar transfer parameters (e.g., Hill 1989), electromagnetic wave propagation in a non-ionized atmosphere (Friehe et al. 1975; Wesley 1976), among others. Here, primed quantities are turbulent excursions from time-averaged variables, and the overbar indicates a time-averaged quantity. While these issues all deserve attention, examining the main mechanisms by which the covariance between two scalar fluctuations is produced, maintained, or dissipated is a legitimate fundamental problem in its own right. Understanding these mechanisms can highlight new dynamical processes modulating the structure of turbulence within the ASL not readily detected by other approaches. In fact, they may even provide blue prints on how to proceed on other practical yet unresolved issues such as the imbalance between available net radiation and the sum of sensible and latent heat fluxes (e.g., Steinfeld et al. 2007).

A number of studies listed in Table 1 have suggested that dissimilarities in the temperature–humidity covariance is often attributed to one (or more) of the following causes: (i) the active roles of temperature (and humidity) in the production/destruction of turbulent kinetic energy, (ii) advection of heat or moisture (both longitudinally and vertically), (iii) unsteadiness in the outer-layer flow that can impinge on the ASL, (iv) source inhomogeneity at the ground surface, and (v) local entrainment processes from the top of the atmospheric boundary layer (ABL). In the upper part of the ABL, the correlation coefficient between heat and water vapour ( $R_{TC}$ ) is generally negative because of the entrainment of warm yet dry air. Hence, it is conceivable that any observed reductions from unity in  $R_{TC}$  within the ASL can be partially explained by this top-down mixing of drier air (see Table 1 for references). Though this latter argument is intuitive and theoretically appealing, the large distance separating the ASL from the entrainment zone, and the ubiquitous presence of other ‘contaminating’ issues (e.g., averaging times and non-stationarity as in Asanuma et al. 2007), make this entrainment argument difficult to establish (see e.g., Andreas et al. 1998; De Bruin et al. 1999).

Progress on the latter point can benefit from an explicit expression that describes how an anti-correlation between temperature and humidity at some level within the ABL propagates down into the ASL. In particular, we seek a simplified expression that predicts how much of the dissimilarity in the temperature–humidity covariance within the ASL originates from a boundary condition above the ASL or from source dissimilarities at the ground, the subject of this study.

**Table 1** Sample studies that reported or discussed covariances and cospectra between temperature and water vapour concentration and possible reasons why their correlation diverges from unity within the atmospheric surface layer

---

*Active roles of temperature (and water vapour)*

---

Flux–gradient (or Roughness) similarity functions: Warhaft (1976), Papaioannou et al. (1989), King and Anderson (1994), Dias and Brutsaert (1996)

Flux–variance similarity functions: Katul and Hsieh (1999)

General turbulence: See Katul and Parlange (1994), Nagata and Komori (2001) for detailed references on active/passive scalars

---

*Advective conditions*

---

Vegetation: Verma et al. (1978), Lang et al. (1983), Wesley (1988), Kroon and De Bruin (1995), McNaughton and Laubach (2000)

Lakes and reservoirs: Assouline et al. (2007)

---

*Modulations from the outer layer (and unsteadiness)*

---

McNaughton and Laubach (1998), McNaughton and Brunet (2002), Högström (1990), Högström et al. (2002), Cullen et al. (2007). The recent analysis in Asanuma et al. (2007) is suggestive that much of the dissimilarity originates at very low frequency (few hours) and can also be interpreted as a result of unsteadiness. Likewise with Phelps and Pond (1971), who attributed this unsteadiness to radiative loading. See also Table in De Bruin et al. (1999) for further discussion

---

*Dissimilarity in ground sources and sinks*

---

Vegetation: Weaver (1990), Padro (1993) who contrasted vegetated surfaces with wetlands; Liu et al. (1998), Kustas et al. (1994), Katul et al. (1995, 1996), Andreas et al. (1998), Asanuma and Brutsaert (1999), Choi et al. (2004), Lamaud and Irvine (2006) demonstrated that the dissimilarity is dependent on the surface Bowen ratio; Williams et al. (2007) demonstrated that the dissimilarity is dependent on leaf area dynamics. The latter two studies do not exclude the possibility of other factors

Urban: Moriwaki and Kanda (2006)

---

*Entrainment processes*

---

LES of a convective boundary layer: Moeng and Wyngaard (1984), Piper et al. (1995)

Vegetation: Mahrt (1991), Mahrt et al. (2001b), De Bruin et al. (1991), De Bruin et al. (1999), Asanuma et al. (2007)

Urban: Roth and Oke (1995), Moriwaki and Kanda (2006)

Marine: Wyngaard et al. (1978), Coulman (1980), Sempreviva and Gryning (2000)

---

Some studies report more than a singular cause

Using a simplified one-dimensional budget model for  $\overline{T'C'}$  that retains production, dissipation, and vertical transport, an analytical solution is proposed that predicts the vertical profile of  $\overline{T'C'}$  from specified boundary conditions just above the ASL and at the ground surface. There are numerous processes that contribute to the  $\overline{T'C'}$  budget not considered here, such as non-stationarity, mean advection, and longitudinal turbulent transport processes, and examining all of them simultaneously is well beyond the scope of a single study. Nevertheless, even in the presence of all these extra processes, the three terms selected here must be retained in the general budget of  $\overline{T'C'}$ .

The marine surface layer is ideal for analyzing such a model because temperature–humidity similarity often exists at (or near) the surface, and advective conditions can be minimized by a suitable choice of wind directions. The lower ‘boundary condition’ imposed on the  $\overline{T'C'}$  budget is less difficult to describe over an extensive water surface, at least when compared to their vegetated or urban canopy surface counterparts. Near vegetated surfaces,  $\overline{T'C'}$  is influenced by complex biological processes, while near urban settings it is influenced by patchy water vapour and heat source distributions that are not spatially co-located.

Observations from RASEX (*Risø Air Sea EXperiment*), collected at an offshore site in Denmark during a campaign in the Autumn of 1994 (Højstrup et al. 1995; Mahrt et al. 1998, 2001a) are used here as a case study. This dataset has the added benefit in that the local production term of the  $\overline{T'C'}$  budget has been studied and shown to scale with surface-layer similarity theory (Sempreviva and Højstrup 1998).

## 2 The RASEX Experiment

Often labelled as the ‘Kansas of the sea’, the RASEX set-up has been described in a number of studies (Højstrup et al. 1995; Sempreviva and Højstrup 1998; Mahrt et al. 1998, 2001a) and only salient features are repeated here for completeness. Data used were collected at a 48-m tower situated offshore in about 4-m water depth but with upstream water depths varying from 5 to 20-m. Two OPHIR hygrometers, mounted at 18 and 32-m, were used for measuring moisture fluctuations, and two Gill Solent sonic anemometers, co-located with the OPHIR instruments, were also used to provide velocity statistics, scalar fluxes, and triple correlations. Data were sampled at 20 Hz and 30-min average statistics were then computed, whilst temperature data from the sonic anemometer were corrected for (1) cross wind speed fluctuations along the skewed sonic path (Schotanus et al. 1983; Kaimal and Gaynor 1991), and (2) transducer shadow effect. The analyses were restricted to winds originating from the sector 230°–360° and 000°–045° ensuring the longest sea fetches.

## 3 Theory

The  $\overline{T'C'}$  budget for a stationary and planar homogeneous flow, in the absence of subsidence, reduces to (e.g., Stull 1988; Garratt 1992; Sempreviva and Højstrup 1998; Juang et al. 2006)

$$\frac{\partial \overline{T'C'}}{\partial t} = 0 = - \left( \overline{w'C'} \frac{\partial \overline{T}}{\partial z} + \overline{w'T'} \frac{\partial \overline{C}}{\partial z} \right) - 2\varepsilon_{TC} - \frac{\partial \overline{w'T'C'}}{\partial z}, \quad (1)$$

where  $T$  and  $C$  are instantaneous air temperature and water vapour concentration, respectively,  $w$  is the instantaneous vertical velocity,  $z$  is the height above the surface,  $t$  is time, and as before, primed quantities are turbulent excursions around their time-averaged states indicated by the overbar. The first term on the right-hand side of Eq. 1 is the production responsible for locally generating the covariance between temperature and humidity; the second is the dissipation rate responsible for the de-correlation between these two scalars, and the third is the flux-transport term responsible for non-local transport of  $\overline{T'C'}$  from other regions in the flow domain.

Using a standard closure model (e.g., Donaldson 1973; Juang et al. 2006) for the dissipation, given by

$$\varepsilon_{TC} = \frac{Q}{\lambda_3} \overline{T'C'}, \quad (2)$$

and for the flux-transport term, given by

$$\overline{w'T'C'} = -Q\lambda_1 \frac{\partial \overline{T'C'}}{\partial z}, \quad (3)$$

Equation 1 reduces to

$$\lambda_1 Q \frac{\partial^2 (\overline{T'C'})}{\partial z \partial z} + \frac{\partial (\lambda_1 Q)}{\partial z} \frac{\partial \overline{T'C'}}{\partial z} - \frac{2}{\lambda_3} Q \overline{T'C'} = \left( \frac{\overline{w'C'}}{\partial z} \frac{\partial \overline{T}}{\partial z} + \overline{w'T'} \frac{\partial \overline{C}}{\partial z} \right), \tag{4}$$

where  $Q = (\overline{u^2} + \overline{v^2} + \overline{w^2})^{1/2}$  is a characteristic turbulent velocity scale,  $u$  and  $v$  are the longitudinal and lateral velocity components, respectively, defined such that  $\bar{v} = 0$ ,  $\lambda_1 = A_1(l_m)$  and  $\lambda_3 = A_3(l_m)$  are related to the canonical mixing length  $l_m$ , and  $A_1$  and  $A_3$  are similarity constants to be determined later.

### 3.1 Simplifications and Analytical Treatment

For analytical tractability, Eq. 4 must be further simplified. In the ASL, these simplifications include:

- (i) The use of a linear  $l_m (= k_v z)$ , where  $k_v$  is Von Karman’s constant.
- (ii) The argument that the local production term in Eq. 4 does not diverge appreciably from surface-layer similarity scaling. Noting that  $\overline{w'C'} = u_* C_*$ ,  $\overline{w'T'} = u_* T_*$ , the mean scalar gradients in the production term are estimated via similarity theory:

$$\frac{\partial \overline{T}}{\partial z} \left( \frac{k_v z}{-T_*} \right) = \phi_T \left( \frac{z}{L} \right), \tag{5a}$$

$$\frac{\partial \overline{C}}{\partial z} \left( \frac{k_v z}{-C_*} \right) = \phi_C \left( \frac{z}{L} \right), \tag{5b}$$

where  $L$  is the Obukhov length, and  $\phi_T$  and  $\phi_c$  are the standard mean gradient stability correction functions.

Hence, with this simplification to the mean scalar gradients, Eq. 4 becomes:

$$\lambda_1 Q \frac{\partial^2 (\overline{T'C'})}{\partial z \partial z} + \frac{\partial (\lambda_1 Q)}{\partial z} \frac{\partial \overline{T'C'}}{\partial z} - \frac{2}{\lambda_3} Q \overline{T'C'} = -\frac{u_* C_* T_*}{k_v z} (\phi_T(z/L) + \phi_c(z/L)) \approx -2 \frac{u_* C_* T_*}{k_v z} \phi_T(z/L). \tag{6}$$

Again, it should be emphasized that  $\phi_T(z/L) \neq \phi_c(z/L)$  for a number of reasons (see Table 1). However, these differences are (a) likely to be smaller than errors introduced by the closure model for the flux-transport or dissipation terms, (b) less significant when compared to the overall vertical variations in  $\overline{T'C'}$ . For reference, it suffices to note that  $\overline{T'C'}/T_* C_*$  can vary from  $-20$  to  $20$  within the convective ABL (Wyngaard et al. 1978). Again, if the differences between  $\phi_T(z/L)$  and  $\phi_c(z/L)$  are known or even vary with  $\overline{T'C'}$ , they can be accounted for, though analytical tractability may become difficult for the latter case.

- (iii) The term

$$\frac{\partial (\lambda_1 Q)}{\partial z} \frac{\partial \overline{T'C'}}{\partial z} = \left( Q \frac{\partial (\lambda_1)}{\partial z} + \lambda_1 \frac{\partial Q}{\partial z} \right) \frac{\partial \overline{T'C'}}{\partial z} \approx A_1 k_v Q \frac{\partial \overline{T'C'}}{\partial z}.$$

This argument is accurate for a near-neutral ASL, but as pure convective conditions are approached, both terms can become significant. As we show later, this assumption is not too restrictive for modelling  $\overline{T'C'}/T_* C_*$  in the lower layers of the ASL.

With these three simplifications, Eq. 6 reduces to:

$$A_1 k_v z Q \frac{\partial^2 \overline{T'C'}}{\partial z \partial z} + A_1 k_v Q \frac{\partial \overline{T'C'}}{\partial z} - \frac{2}{A_3 k_v z} Q \overline{T'C'} = -2C_* T_* u_* \frac{\phi_T(z/L)}{k_v z}, \tag{7}$$

and upon multiplying by  $z$  and dividing by  $A_1 k_v Q$ , this reduces to:

$$z^2 \frac{\partial^2 \overline{T'C'}}{\partial z \partial z} + z \frac{\partial \overline{T'C'}}{\partial z} - \frac{2}{A_3 A_1 k_v^2} \overline{T'C'} = -2C_* T_* \left( \frac{u_*}{Q} \right) \frac{\phi_T(z/L)}{A_1 k_v^2}. \tag{8}$$

Noting that  $Q/u_* = \sqrt{2\phi_{TKE}}$ , where  $\phi_{TKE}$  is the stability correction function for the turbulent kinetic energy (TKE), Eq. 8 can now be expressed in dimensionless form as:

$$z^2 \frac{\partial^2 (\overline{T'C'}/C_* T_*)}{\partial z \partial z} + z \frac{\partial (\overline{T'C'}/C_* T_*)}{\partial z} - \left( \frac{2}{A_3 A_1 k_v^2} \right) \frac{\overline{T'C'}}{C_* T_*} = - \left( \frac{2}{A_1 k_v^2} \right) \frac{\phi_T}{\sqrt{2\phi_{TKE}}}. \tag{9}$$

In Eq. 9, when  $\frac{\partial \overline{w'T'C'}}{\partial z} = 0$ , or production balances the dissipation rate, the covariance budget equation becomes

$$\frac{\overline{T'C'}}{C_* T_*} = A_3 \frac{\phi_T}{\sqrt{2\phi_{TKE}}}, \tag{10}$$

and scales with  $z/L$  if  $\phi_{TKE}$  only scales with  $z/L$  or both  $z/L$  and  $z_i/L$  (where  $z_i$  is the boundary-layer height), as discussed in Hsieh and Katul (1997).

### 3.2 Homogeneous and General Solutions

Equation 9 is a non-homogeneous Cauchy–Euler equation of the form

$$z^2 \frac{d^2 y}{dz^2} + z \frac{dy}{dz} - ay = r(z), \tag{11}$$

where  $y = \frac{\overline{T'C'}}{T_* C_*}$ ,  $a = \frac{2}{A_3 A_1 k_v^2} > 0$ , and  $r(z) = - \left( \frac{2}{A_1 k_v^2} \right) \frac{\phi_T}{\sqrt{2\phi_{TKE}}}$ , and whose homogeneous solution (i.e., when  $r(z) = 0$ , or physically when the  $\overline{T'C'}$  budget is expressed without the local production term) is given by

$$y_h(z) = B_1 z^{\sqrt{a}} + B_2 z^{-\sqrt{a}}. \tag{12}$$

When  $z \rightarrow 0$ , the homogeneous solution is governed by  $y_h(z) \rightarrow B_2 z^{-\sqrt{a}}$ , and when  $z \rightarrow +\infty$ ,  $y_h(z) \rightarrow B_1 z^{\sqrt{a}}$ . In short, these two homogeneous solutions can be interpreted as indicators of how variations in the upper and lower boundary conditions affect the normalized  $\overline{T'C'}$  values at a given height in the ASL. Physically, if a boundary condition injects a finite  $\overline{T'C'}$  (whether from the top or the bottom of the flow domain), the homogeneous solution describes the interplay between its transport away from the boundary and its eventual dissipation in the absence of local production.

To account for this local production, a particular adjustment to  $y_h$  is necessary. To derive this particular adjustment, we note that the Wronskian ( $= Wr(y_1, y_2)$ ) of these two homogeneous solutions (i.e.,  $y_1 = z^{\sqrt{a}}$ ,  $y_2 = z^{-\sqrt{a}}$ ) is

$$\begin{aligned} Wr(y_1, y_2) &= \begin{vmatrix} y_1 & y_2 \\ \frac{dy_1}{dz} & \frac{dy_2}{dz} \end{vmatrix} \\ &= \begin{vmatrix} z^{\sqrt{a}} & z^{-\sqrt{a}} \\ \sqrt{a} z^{\sqrt{a}-1} & -\sqrt{a} z^{-\sqrt{a}-1} \end{vmatrix} = -\sqrt{a} z^{-1} - \sqrt{a} z^{-1} = \frac{-2\sqrt{a}}{z} \neq 0. \end{aligned} \tag{13}$$

A finite Wronskian is suggestive that the ‘*Method of Variation of Parameters*’ can be used to infer this particular solution ( $y_p$ ) and correct for  $r(z) \neq 0$ . The general solution can then be expressed as

$$y(z) = y_h(z) + y_p(z), \tag{14}$$

where  $y_p = f_1(z)z^{\sqrt{a}} + f_2(z)z^{-\sqrt{a}}$ ,  $f_1 = -\int \frac{z^{-\sqrt{a}}r(z)}{W_r(z)} dz$ ,  $f_2 = \int \frac{z^{\sqrt{a}}r(z)}{W_r(z)} dz$ . Hence, the final solution is given by

$$\frac{T'C'}{T_*C_*} = \left[ B_1 + \frac{1}{2\sqrt{a}} \int z^{1-\sqrt{a}} r(z) dz \right] z^{\sqrt{a}} + \left[ B_2 - \frac{1}{2\sqrt{a}} \int z^{1+\sqrt{a}} r(z) dz \right] z^{-\sqrt{a}}, \tag{15a}$$

$$\equiv B_3(L) z^{\sqrt{a}} + B_4(L) z^{-\sqrt{a}} \tag{15b}$$

where

$$B_3(L) = B_1 + \left( \frac{-1}{A_1 k_v^2} \right) \frac{1}{\sqrt{\frac{2}{A_3 A_1 k_v^2}}} \int \left( z^{1-\sqrt{\frac{2}{A_3 A_1 k_v^2}}} \frac{\phi_T(z/L)}{\sqrt{2} \phi_{TKE}(z/L)} \right) dz, \tag{16a}$$

$$B_4(L) = B_2 + \left( \frac{1}{A_1 k_v^2} \right) \frac{1}{\sqrt{\frac{2}{A_3 A_1 k_v^2}}} \int \left( z^{1+\sqrt{\frac{2}{A_3 A_1 k_v^2}}} \frac{\phi_T(z/L)}{\sqrt{2} \phi_{TKE}(z/L)} \right) dz. \tag{16b}$$

Note in Eq. 16 that, because the integration is carried out over  $z$ ,  $B_3$  and  $B_4$  vary only with  $L$  once the closure constants are specified. The values of  $B_1$  and  $B_2$  must be evaluated from the boundary conditions specified near the ground and near the top of the ASL. Equation 15 still maintains that the impact of the two boundary conditions is asymmetric—the influence of the upper boundary condition tends to scale as  $z^{\sqrt{a}}$  and its contribution diminishes as the surface is approached, while the influence of the lower boundary condition tends to scale as  $z^{-\sqrt{a}}$ , and its influence rapidly diminishes with increasing  $z$ . The integrals in Eq. 15, whose genesis are local production terms that primarily vary with  $L$  (though the height of the ABL can be accounted for in  $r(z)$  via  $\phi_{TKE}$ ), and that can be evaluated analytically. However, their general expression leads to hyper-geometric functions (expressed as series expansion) that are neither explicit nor intuitive in demonstrating how  $L$  modifies  $B_3$  or  $B_4$ .

Hence, for practical calculations, numerical integration of Eq. 9 is actually as convenient as a numerical integration of  $B_3$  and  $B_4$ , and hereafter, we refer to this numerical solution as the model solution. Again, the main advantage of the analytical expression here is not computational but is intended to discern how the influences of the upper and lower boundary conditions propagate with  $z$  within the ASL.

### 4 Results

To address the study objectives, it is necessary to (i) estimate the two similarity constants  $A_1$  and  $A_3$ , (ii) explore how well the gradient–diffusion closure assumption reproduces the triple moments, and (iii) evaluate the overall performance of the analytical model within the ASL and its robustness to various simplifications.

### 4.1 Determination of the Similarity Constants

For matching the ASL diffusivity under ideal conditions,  $\lambda_1 Q = (A_1 k_v z) Q = k_v z u_*$ , and hence

$$A_1 = \frac{1}{\sqrt{\frac{1}{2} (A_u^2 + A_v^2 + A_w^2)}}, \tag{17}$$

where, for near-neutral conditions,  $A_u = \sigma_u/u_* \approx 2.7$ ,  $A_v = \sigma_v/u_* \approx 2.1$ , and  $A_w = \sigma_w/u_* \approx 1.25$  resulting in an estimated  $A_1 \approx 0.39$ .

To determine  $A_3$ , recall that when  $\frac{\partial \overline{T'C'}}{\partial z} = 0$

$$\frac{\overline{T'C'}}{C_* T_*} = A_3 \frac{\phi_T}{\sqrt{2\phi_{TKE}}}, \tag{17a}$$

and

$$\frac{\overline{T'C'}}{C_* T_*} \frac{1}{\frac{\sigma_T}{T_*} \frac{\sigma_c}{C_*}} = R_{TC} = A_3 \left( \frac{\phi_T}{\sqrt{2\phi_{TKE}}} \right) \frac{1}{\phi_{TT}\phi_{cc}}. \tag{17b}$$

Here,  $\sigma_s = \left( \overline{s's'} \right)^{1/2}$  is the standard deviation of an arbitrary flow variable  $s$ , and  $\sigma_T/T_* = \phi_{TT}$  and  $\sigma_c/C_* = \phi_{cc}$  are the scalar variance stability correction functions. A maximum  $A_3 \approx 5.3$  ensures  $|R_{TC}| \leq 1$  (see Fig. 1) when using standard surface-layer similarity theory functions for  $\phi_T$  and  $\phi_{TKE}$  (formulations are presented in Hsieh and Katul 1997 and are not repeated here), and for  $\phi_{TT}$  and  $\phi_{cc}$  (formulations are presented in Sorbjan 1989, Table 4.2 after Tillman 1972). It should be emphasized that  $A_3 = 5.3$  is dependent on the choice of  $\phi_T$ ,  $\phi_{TKE}$ ,  $\phi_{TT}$  and  $\phi_{cc}$ , and cannot be treated as a ‘universal’ closure constant.

### 4.2 The Effects of Atmospheric Stability on $\overline{T'C'}$ and its Budget

Using these two similarity constants, Fig. 2 illustrates how the upper boundary condition, fixed here at  $\overline{T'C'}/(T_* C_*) = -2$ , affects the vertical distribution of  $\overline{T'C'}/(T_* C_*)$  assuming  $\partial \overline{T'C'}/\partial z = 0$  at  $z = 0$  as  $L$  varies. These model calculations were conducted by assuming the maximum ASL height  $z_{\max} = 100$  m (i.e., some 10% of the mixed-layer height), and the value  $\overline{T'C'}/(T_* C_*) = -2$  was set at 10% of the maximum value near the top of the mixed layer (e.g. Wyngaard et al. 1978), and *purposely* chosen as *negative* to initiate a dissimilarity between heat and water vapour at  $z_{\max}$ . In reality, data from Wyngaard et al. (1978) suggest that  $\overline{T'C'}/(T_* C_*) = -2$  occurs around the middle of the convective boundary layer (depth  $h_{cbl}$ ) or at  $z = 0.5h_{cbl}$ . The top of the ASL is usually around 10–20% of  $h_{cbl}$ .

It is clear that, for near-convective conditions, this boundary condition propagates ‘deeper’ into the domain when compared to the near-neutral atmospheric stability state. This propagation is perhaps most evident by the height at which  $\overline{T'C'}$  crosses the zero value and reverses sign. For near convective conditions, the ‘zero crossing’ occurs closer to the ground, while for near-neutral conditions, the zero crossing occurs almost mid-way in the domain. Note that the production function of  $\overline{T'C'}$ , also shown in Fig. 2, suggests that for near-neutral atmospheric conditions, its decay is much slower with increasing  $z$  when compared to its convective counterpart. Figure 2 shows that near the surface ( $z/z_{\max} < 0.2$ ), the  $\overline{T'C'}$  budget is mainly governed by a balance between production and dissipation as expected, but near the top of the domain (around 100 m), the flux-transport term becomes significant.

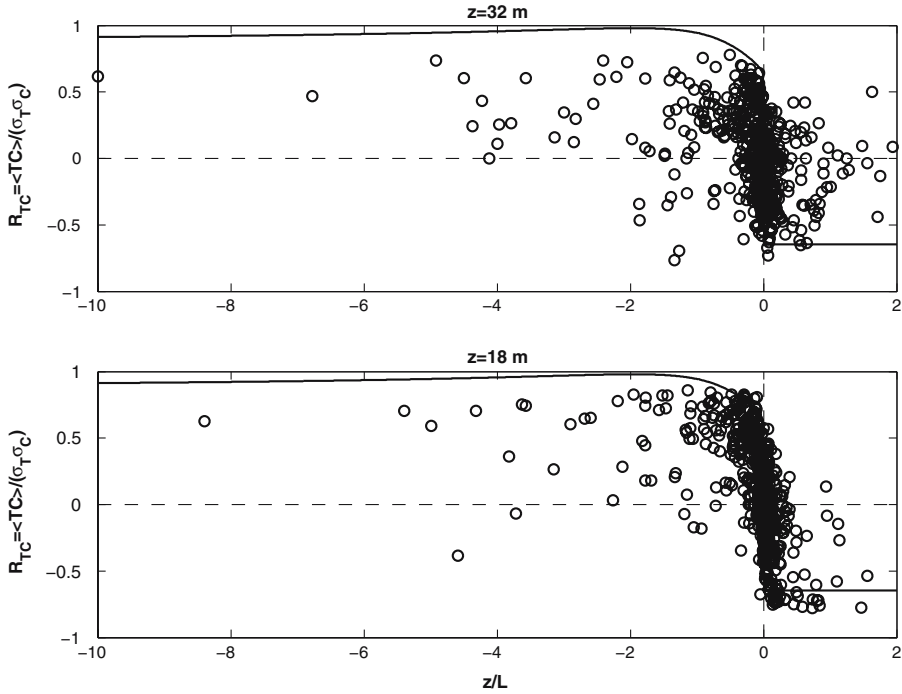


**Fig. 1** The variation of the correlation coefficient between temperature and water vapour ( $R_{TC}$ ) with the stability parameter ( $z/L$ ). Measured  $R_{TC}$  in open circles at  $z = 32\text{ m}$  (top) and  $z = 18\text{ m}$  (bottom) from the RASEX are shown. The solid line reflects a balance between production and dissipation resulting in  $R_{TC} = A_3 \left( \frac{\phi_T}{\sqrt{2}\phi_{TKE}} \right) \frac{1}{\phi_{TT}\phi_{cc}}$  with  $A_3 = 5.3$

### 4.3 Gradient–Diffusion Closure Assumption

Because of the availability  $\overline{T'C'}$  and  $\overline{w'C'T'}$  at two levels, the closure assumption for the triple moment, given by

$$\overline{w'T'C'} = -A_1 k_v z Q \frac{\partial \overline{T'C'}}{\partial z} \tag{18}$$

can be directly evaluated. Figure 3 shows the comparison between measured and modelled  $\overline{w'C'T'}$ . Here, measured  $\overline{w'C'T'}$  as well as measured  $Q$  were computed by averaging the values at the two levels for each run (thus,  $z = 25\text{ m}$  is set in the diffusivity calculation), while the gradient in  $\overline{T'C'}$  was computed by differencing the measured values at the two levels. The comparison in Fig. 3 suggests that such an approximation has some predictive skills, but leaves much to be desired in the performance of a general closure model. In particular, for small magnitudes of  $\overline{w'C'T'}$ , the gradient–diffusion approximation fails to predict the sign of the triple moment. This failure may be due to a number of factors, including measurement errors of the differences in  $\overline{T'C'}$  (as well as the finite difference approximation of  $\partial \overline{T'C'} / \partial z$ ), sampling errors, and instrumentation errors (including instrument separation). Whether this failure significantly degrades the model performance is explored next. However, before exploring this point, we note that the modelled  $\overline{T'C'}$  is likely to be more robust to these issues than the modelled  $\overline{w'C'T'}$  for two reasons:

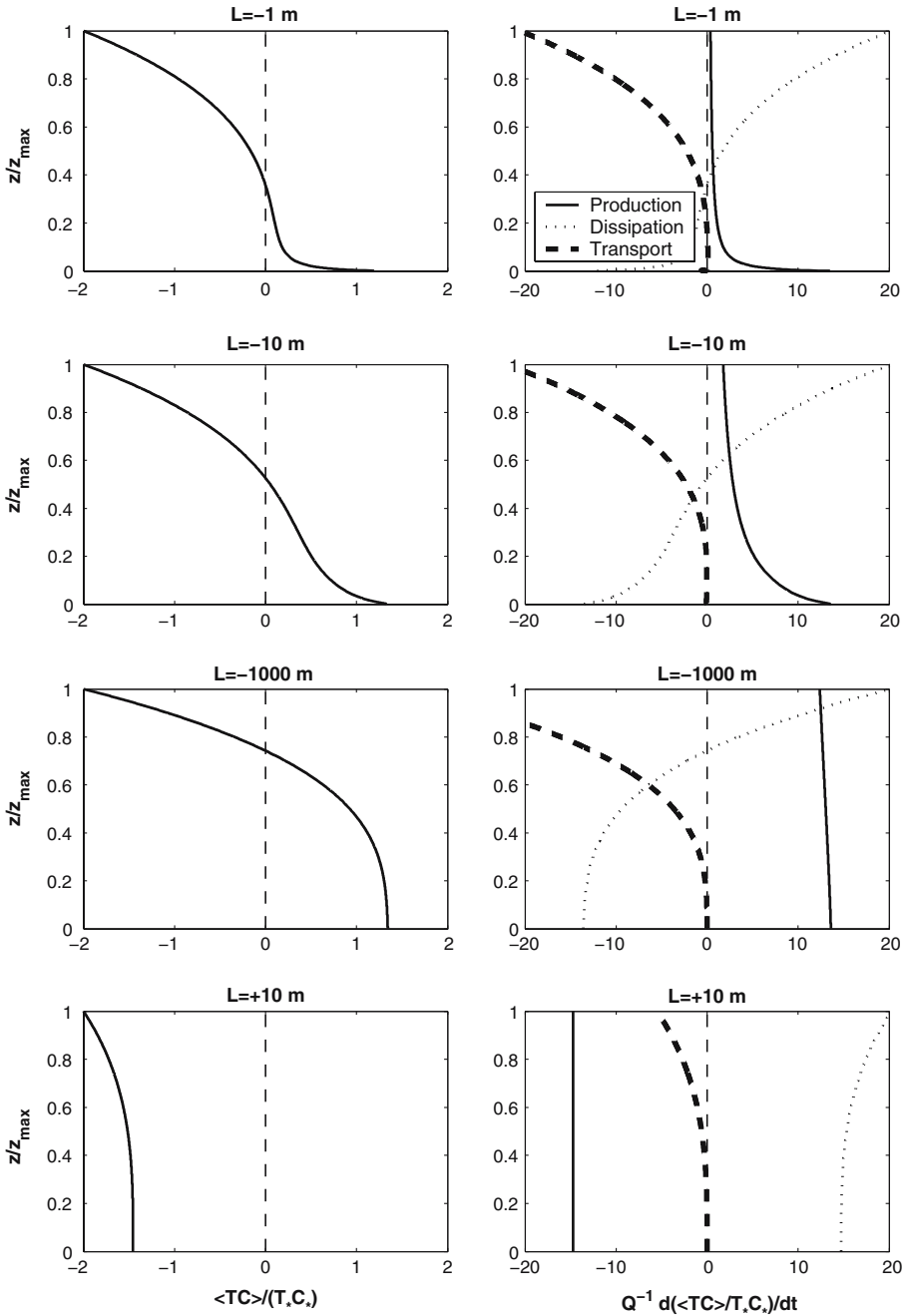


**Fig. 2** The variations of  $\overline{T'C'}/T_*C_*$  (left) and the three budget terms (right)—production (solid line), transport (dashed), and dissipation (dot-dashed). Here,  $z_{\max}$  is the domain depth (=100 m), and the values of  $L$  were chosen to span convective to mildly stable atmospheric stability conditions

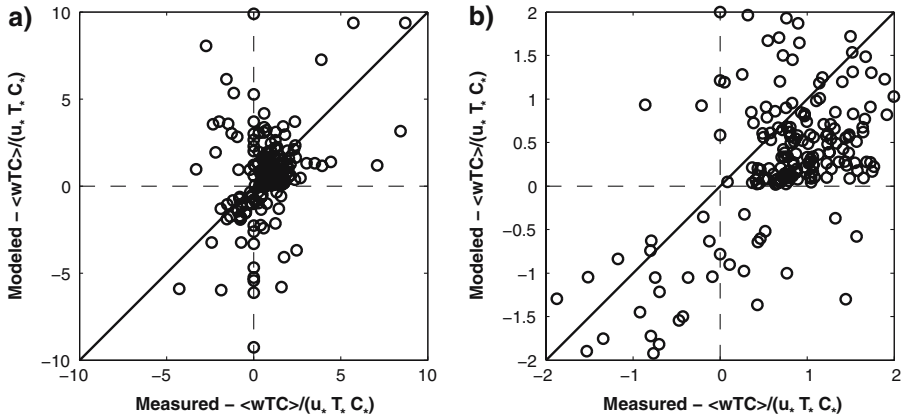


**Fig. 3** (a) Comparison between measured and modelled normalized triple moments. The 1:1 line is shown. (b) Same as panel (a) but for small variations in the triple moments. Note that while the majority of the points fall below the 1:1 line, yet their variations do not diverge appreciably from a 1:1 behaviour

- (i) The  $\overline{T'C'}$  model is sensitive to gradients in  $\overline{w'C'T'}$ , not their absolute magnitude. In other words, offsets between measured and modelled  $\overline{w'C'T'}$  become less important as long as the relationship between measured and modelled triple moment maintains a near 1:1 slope.
- (ii) The flux transport term remains smaller than the production or dissipation terms within the surface layer (where the RASEX data were collected). Hence, accounting for the flux-transport term, rather than ignoring it, remains the first-order correction in the  $\overline{T'C'}$  budget.

#### 4.4 Model Evaluation

Since  $\overline{T'C'}$  just above the ASL is not known, the model testing here is less than ideal. The covariance  $\overline{T'C'}$  measured at 32 m can be used as an upper boundary condition in the model to infer  $\overline{T'C'}$  at 18 m assuming that  $\partial\overline{T'C'}/\partial z = 0$  at the surface. This lower boundary condition eliminates the need to describe  $\overline{T'C'}$  at the surface, which can be difficult in the presence of wave generation and breaking (e.g., [Sjoblom and Smedman 2003](#)). If known, including it in place of  $\partial\overline{T'C'}/\partial z = 0$  at  $z=0$  can be readily incorporated in the proposed approach. Agreement between measured and modelled  $\overline{T'C'}$  at 18 m serves as a reasonable (yet indirect) test of the robustness the model to assumptions, simplifications, and failures of the gradient–diffusion closure shown in Fig. 3. More important in this evaluation is the information introduced by the model about variations in  $\overline{T'C'}$  at 18 m beyond that already measured at 32 m. Hence, the comparison presented in Fig. 4 is displayed with the abscissa being  $\overline{T'C'}/(T_*C_*)$  measured at 32 m while the ordinate has the measured and modelled  $\overline{T'C'}/(T_*C_*)$  at  $z = 18$  m. The 1:1 line is the outcome of a hypothetical ‘dummy’ model that transmits from 32 m down to 18 m without any alteration. Departures from the 1:1 line signify added information by the model about the behaviour of  $\overline{T'C'}/(T_*C_*)$  at  $z = 18$  m beyond variations in this upper boundary condition. It is clear from Fig. 4 that the analytical model explains reasonably well the main departures from the 1:1 line, suggesting that the model can explain variations in  $\overline{T'C'}/(T_*C_*)$  at  $z = 18$  m beyond that provided by the boundary condition forcing at  $z = 32$  m (except when  $\overline{T'C'}/(T_*C_*)$  at  $z = 32$  m is small). Another

**Fig. 4** Comparison between measured (*plus*) and modelled  $\overline{T'C'}/T_*C_*$  (*open circle*) at  $z = 18$  m. Note that model departure from the 1:1 line (*solid*) is the information generated by the model on  $\overline{T'C'}/T_*C_*$  variation at  $z = 18$  m beyond the variations imposed by the measured boundary condition at  $z = 32$  m (*abscissa*)

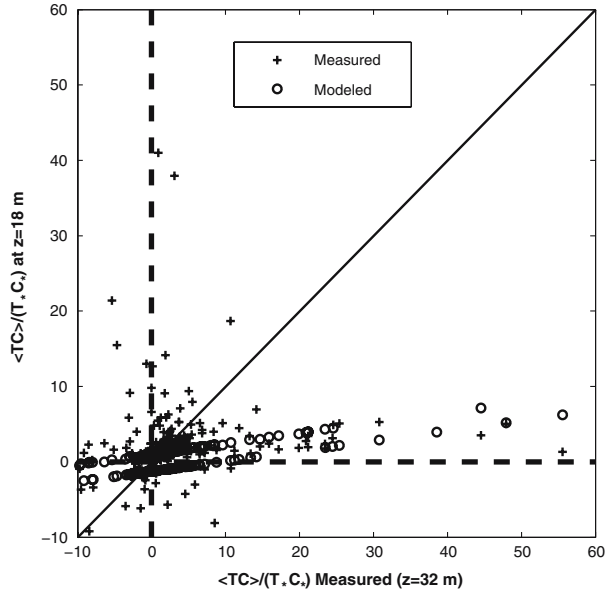
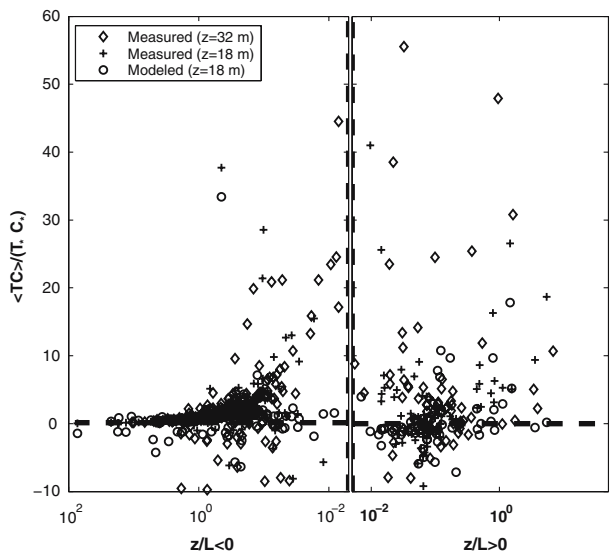


**Fig. 5** Variations of  $\overline{T'C'}/T_*C_*$  with  $z/L$  for the RASEX data showing that the large values and scatter are mostly for near-neutral runs



point worthy of mentioning is that much of the large  $\overline{T'C'}/(T_*C_*)$  and the concomitant large scatter are for the near-neutral regimes (i.e., where  $\partial Q/\partial z \rightarrow 0$ ) as shown in Fig. 5. As convective conditions are approached (i.e., where  $\partial Q/\partial z \neq 0$ ),  $\overline{T'C'}/(T_*C_*)$  decays rapidly (as was also shown in Coulman 1980), a fortunate outcome given the simplification

$$\frac{\partial (\lambda_1 Q)}{\partial z} \frac{\partial \overline{T'C'}}{\partial z} \approx A_1 k_v Q \frac{\partial \overline{T'C'}}{\partial z}.$$

## 5 Discussion and Conclusions

A simplified analytical model that predicts how much of the temperature–humidity covariance within the ASL originates just above the ASL and from the surface is proposed. The model is based on a simplified budget for  $\overline{T'C'}$  that retains three basic terms: production, dissipation, and vertical transport. In the absence of any other local definitive data, the production term was assumed to follow similarity theory scaling though this assumption is not necessary if mean temperature and mean humidity profiles are available. Standard second-order closure formulations were adopted for the triple moments and the dissipation terms, and the canonical mixing length for the closure model was assumed to be linear with height from the surface. Despite the poor performance of the gradient–diffusion closure assumption characterizing the triple moment, the overall model was shown to be sufficiently robust in reproducing  $\overline{T'C'}/(T_*C_*)$  from known  $\overline{T'C'}/(T_*C_*)$  at some higher level. This result can guide interpretations of specific field data with regards to the role of entrainment processes near the land surface. Starting with a  $\overline{T'C'}/(T_*C_*)$  measured above the surface, it is possible to predict the value of  $\overline{T'C'}/(T_*C_*)$  at the top of the surface layer (say at 200 m) assuming  $\partial\overline{T'C'}/\partial z = 0$  at  $z = 0$ , and ask whether this estimate is plausible when compared to the Wyngaard et al. (1978) data for a convective boundary layer (CBL).

One of the main findings from the analytical treatment here regards the asymmetry on how the top and bottom boundary conditions affect the  $\overline{T'C'}/(T_*C_*)$  in the ASL. This asymmetry resembles the so-called ‘top-down’ and ‘bottom-up’ diffusion extensively studied in the CBL. For example, both laboratory experiments and large-eddy simulation (LES) results indicate that when a scalar is introduced into the bottom of the CBL with no flux through the top (referred to as bottom-up diffusion), its diffusivity profile radically differs from a scalar introduced at the CBL top with zero flux at the surface (referred to as top-down diffusion) (e.g., Wyngaard and Brost 1984; Moeng and Wyngaard 1984; Piper et al. 1995). The proposed analytical solution here suggests that within the ASL, variations in  $\overline{T'C'}/(T_*C_*)$  at the surface propagate upward in the ASL differently from variations in  $\overline{T'C'}/(T_*C_*)$  originating from the top of the ASL. This asymmetry (i.e., bottom-up scaling is  $z^{-\sqrt{a}}$  while top-down scaling is  $z^{\sqrt{a}}$ ) was shown not to originate only from vertical inhomogeneity in the local production function or atmospheric stability. Rather, its genesis stems from the flux-transport term, the basis of the second-order term in the Cauchy–Euler equation. Even in the absence of any inhomogeneity in the local production function within the ASL, the asymmetry in  $\overline{T'C'}/(T_*C_*)$  profile persists through the homogeneous solution.

There are a number of generalizations that can be implemented within this model framework—for example, by revising the local production term to include both surface-layer and mixed-layer similarity scaling and concomitantly revising the canonical mixing length to include both  $z$  and mixed-layer height. These revisions, while they do not affect the homogeneous solution, can permit direct calculations of how dissimilarity at the top of the capping inversion propagates down to the surface, although knowledge of the mixed layer height is required. Hence, the findings here do not provide ‘finality’ to the covariance between humidity and temperature or the entrainment arguments (see Table 1). Rather, they are intended to initiate new hypotheses about the role of entrainment in the  $\overline{T'C'}/(T_*C_*)$  budget (see Table 1) and invite future high-resolution LES experiments that can track such asymmetry and explore optimum closure schemes for the flux-transport and dissipative term.

**Acknowledgements** G. Katul acknowledges support from the National Science Foundation (NSF-EAR 06-35787 and NSF-EAR-06-28432), the United States–Israel Binational Agricultural Research and Development

(BARD, Research Grant No. IS3861-06), and the US Department of Energy (DOE) through the office of Biological and Environmental Research (BER) Terrestrial Carbon Processes (TCP) program (Grants # 10509-0152, DE-FG02-00ER53015, and DE-FG02-95ER62083). D. Cava acknowledges the Italian MIUR Project: ‘Sviluppo di un Sistema Integrato Modellistica Numerica-Strumentazione e Tecnologie Avanzate per lo Studio e le Previsioni del Trasporto e della Diffusione di Inquinanti in Atmosfera’, grant “Bando 1105/2002 project n. 245”.

## References

- Andreas EL, Hill RJ, Gosz JR, Moore DI, Otto WD, Sarma AD (1998) Statistics of surface-layer turbulence over terrain with meter-scale heterogeneity. *Boundary-Layer Meteorol* 86:379–408
- Asanuma J, Brutsaert W (1999) Turbulence variance characteristics of temperature and humidity in the unstable atmospheric surface layer above a variable pine forest. *Water Resour Res* 35:515–521
- Asanuma J, Tamagawa I, Ishikawa H, Ma Y, Hayashi T, Qi Y, Wang J (2007) Spectral similarity between scalars at very low frequencies in the unstable atmospheric surface layer over the Tibetan plateau. *Boundary-Layer Meteorol* 122:85–103
- Assouline S, Tyler S, Tanny J, Cohen S, Bou-Zeid E, Parlange MB, Katul GG (2007) Evaporation from three water bodies of different sizes and climates: measurements and scaling analysis. *Adv Water Resour* (to appear)
- Choi T, Kim J, Lee H, Hong J, Asanuma J, Ishikawa H, Gao Z, Wang J, Koike T (2004) Turbulent exchange of heat, water vapour and momentum over a Tibetan prairie by eddy covariance and flux-variance measurements. *J Geophys Res Atmos* 109(D21):D21106
- Coulman CE (1980) Correlation between velocity, temperature and humidity fluctuations in the air above land and ocean. *Boundary-Layer Meteorol* 19:403–420
- Cullen NJ, Steffen K, Blanken PD (2007) Nonstationarity of turbulent heat fluxes at Summit, Greenland. *Boundary-Layer Meteorol* 122:439–455
- De Bruin HAR, Bink NI, Kroon LJM (1991) Fluxes in the surface layer under advective conditions. In: Schmugge TJ, Andre JC (eds) *Workshop on land surface evaporation measurement and parameterization*. Springer-Verlag, New York pp 157–169
- De Bruin HAR, Van Der Hurk JJM, Kroon LJM (1999) On the temperature–humidity correlation and similarity. *Boundary-Layer Meteorol* 93:453–468
- Dias N, Brutsaert W (1996) Similarity of scalars under stable conditions. *Boundary-Layer Meteorol* 80:355–373
- Donaldson C (1973) Construction of a dynamic model of the production of atmospheric turbulence and the dispersal of atmospheric pollutants. In: Haugen D (ed) *Workshop on micrometeorology*. American Meteorological Society, Boston pp 313–392
- Friehe C, LaRue J, Champagne F, Gibson C (1975) Effects of temperature and humidity fluctuations on the optical refractive index in the marine boundary layer. *J Opt Soc Am* 65:1502–1511
- Garratt JR (1992) *The atmospheric boundary layer*. Cambridge University Press, UK 316 pp
- Hill RJ (1989) Implications of Monin–Obukhov similarity theory for scalar quantities. *J Atmos Sci* 46:2236–2244
- Högström U (1990) Analysis of turbulence structure in the surface layer with a modified similarity formulation for near neutral conditions. *J Atmos Sci* 47:1949–1972
- Högström U, Hunt JCR, Smedman AS (2002) Theory and measurements for turbulence spectra and variances in the atmospheric neutral surface layer. *Boundary-Layer Meteorol* 103:101–124
- Højstrup J, Edson JB, Hare JE, Courtney MS, Sanderhoff P (1995) The RASEX 1994 experiments Risø-R-788. Risø National Laboratory, DK4000 Roskilde, Denmark
- Hsieh CI, Katul GG (1997) Dissipation methods, Taylor’s hypothesis, and stability correction functions in the atmospheric surface layer. *J Geophys Res Atmos* 102(D14):16391–16405
- Juang J-Y, Katul GG, Siqueira MB, Stoy PC, Palmroth S, McCarthy HR, Kim H-S, Oren R (2006) Modeling nighttime ecosystem respiration from measured CO<sub>2</sub> concentration and air temperature profiles using inverse methods. *J Geophys Res* 111, D08S05. DOI:10.1029/2005JD005976
- Kaimal JC, Gaynor JE (1991) Another look at the sonic anemometry. *Boundary-Layer Meteorol* 56:401–410
- Katul GG, Hsieh C-I (1999) A note on the flux-variance similarity relationship for heat and water vapour in the unstable atmospheric surface layer. *Boundary-Layer Meteorol* 90:327–338
- Katul GG, Parlange MB (1994) On the active role of temperature in surface layer turbulence. *J Atmos Sci* 51:2181–2195

- Katul GG, Goltz SM, Hsieh C-I, Cheng Y, Mowry F, Sigmon J (1995) Estimation of surface heat and momentum fluxes using the flux-variance method above uniform and non-uniform terrain. *Boundary-Layer Meteorol* 74:237–260
- Katul GG, Hsieh C-I, Oren R, Ellsworth D, Phillips N (1996) Latent and sensible heat flux predictions from a uniform pine forest using surface renewal and flux-variance methods. *Boundary-Layer Meteorol* 80:249–282
- King JC, Anderson PS (1994) Heat and water-vapor fluxes and scalar roughness lengths over an Antarctic ice shelf. *Boundary-Layer Meteorol* 69:101–121
- Kroon LJM, De Bruin HAR (1995) The Crau field experiment: turbulent exchange in the surface layer under conditions of strong local advection. *J Hydrol* 166:327–351
- Kustas W, Blanford J, Stannard D, Daughtry C, Nichols W, Weltz M (1994) Local energy flux estimates for unstable conditions using variance data in semiarid rangelands. *Water Resour Res* 30:1351–1361
- Lamaud E, Irvine M (2006) Temperature–humidity dissimilarity and heat-to-water-vapour transport efficiency above and within a pine forest canopy: the role of the Bowen ratio. *Boundary-Layer Meteorol* 120(1):87–109
- Lang A, McNaughton KG, Fazu C, Bradley E, Ohtaki E (1983) Inequality of eddy transfer-coefficients for vertical transport of sensible and latent heats during advective inversions. *Boundary-Layer Meteorol* 25:25–41
- Liu XH, Tsukamoto O, Oikawa T, Ohtaki E (1998) A study of correlations of scalar quantities in the atmospheric surface layer. *Boundary-Layer Meteorol* 87:499–508
- Mahrt L (1991) Boundary-layer moisture regimes. *Quart J Roy Meteorol Soc* 117:151–176
- Mahrt L, Vickers D, Edson J, Sun J, Højstrup J, Hare J, Wilczak J (1998) Heat flux in the coastal zone. *Boundary-Layer Meteorol* 86:421–446
- Mahrt L, Vickers D, Edson J, Wilczak J, Hare J, Højstrup J (2001a) Vertical structure of turbulence in offshore flow during RASEX. *Boundary-Layer Meteorol* 180:265–279
- Mahrt L, Vickers D, Sun J (2001b) Spatial variations of surface moisture flux from aircraft data. *Adv Water Resour* 24:1133–1141
- McNaughton KG, Brunet Y (2002) Townsend’s hypothesis, coherent structures and Monin–Obukhov Similarity. *Boundary-Layer Meteorol* 102:161–175
- McNaughton KG, Laubach J (1998) Unsteadiness as a cause of non-equality of eddy diffusivities for heat and vapour at the base of an advection inversion. *Boundary-Layer Meteorol* 88:479–504
- McNaughton KG, Laubach J (2000) Power spectra and cospectra for wind and scalars in a disturbed surface layer at the base of an advective inversion. *Boundary-Layer Meteorol* 96:143–185
- Moeng CH, Wyngaard JC (1984) Statistics of conservative scalars in the convective boundary layer. *J Atmos Sci* 41:3161–3169
- Moriwaki R, Kanda M (2006) Local and global similarity in turbulent transfer of heat, water vapour, and CO<sub>2</sub> in the dynamic convective sublayer over a suburban area. *Boundary-Layer Meteorol* 120:163–179
- Nagata K, Komori S (2001) The difference in turbulent diffusion between active and passive scalars in stable thermal stratification. *J Fluid Mech* 430:361–380
- Padro J (1993) An investigation of flux-variance methods and universal functions applied to three land-use types in unstable conditions. *Boundary-Layer Meteorol* 66:413–425
- Papaioannou G, Jacovides C, Kerkides P (1989) Atmospheric stability effects on eddy transfer coefficients and on Penman’s evaporation estimates. *Water Resour Manag* 3:315–322
- Phelp GT, Pond S (1971) Spectra of temperature and humidity fluctuations and of humidity fluxes and sensible heat flux in a marine boundary-layer. *J Atmos Sci* 28:918–928
- Piper M, Wyngaard JC, Snyder WH, Lawson R (1995) Top-down, bottom-up diffusion experiments in a water convection tank. *J Atmos Sci* 52:3607–3619
- Roth M, Oke T (1995) Relative efficiencies of turbulent transfer of heat, mass, momentum over a patchy urban surface. *J Atmos Sci* 52:1863–1874
- Schotanus P, Nieuwstadt FTM, De Bruin HAR (1983) Temperature measurement with a sonic anemometer and its application to heat and moisture fluxes. *Boundary-Layer Meteorol* 26:81–93
- Sempreviva AM, Gryning SE (2000) Mixing height over water and its role on the correlation between temperature and humidity fluctuations in the unstable surface layer. *Boundary-Layer Meteorol* 97:273–291
- Sempreviva AM, Højstrup J (1998) Transport of temperature and humidity variance and covariance in the marine surface layer. *Boundary-Layer Meteorol* 87:233–253
- Sjoblom A, Smedman AS (2003) Vertical structure in the marine atmospheric boundary layer and its implication for the inertial dissipation method. *Boundary-Layer Meteorol* 109:1–25
- Sorbjan Z (1989) *Structure of the atmospheric boundary layer*. Prentice Hall, Englewood Cliff, NJ, 317 pp

- Steinfeld G, Letzel MO, Raasch S, Kanda M, Inagaki A (2007) Spatial representativeness of single tower measurements and the imbalance problem with eddy-covariance fluxes: results of a large-eddy simulation study. *Boundary-Layer Meteorol* 123(1):77–98
- Stull R (1988) *An introduction to boundary layer meteorology*. Kluwer Academic Press, 666 pp
- Tillman JE (1972) The indirect determination of stability, heat and momentum fluxes in the atmospheric boundary layer from simple scalar variables during dry unstable conditions. *J Appl Meteorol* 11:783–792
- Verma S, Rosenberg B, Blad BL (1978) Turbulent exchange coefficients for sensible heat and water vapour under advective conditions. *J Appl Meteorol* 17:303–338
- Warhaft Z (1976) Heat and moisture fluxes in the stratified boundary layer. *Quart J Roy Meteorol Soc* 102:703–706
- Weaver HJ (1990) Temperature and humidity flux–variances relations determined by one-dimensional eddy-correlation. *Boundary-Layer Meteorol* 53:77–91
- Wesley ML (1976) Combined effect of temperature and humidity fluctuations on refractive index. *J Appl Meteorol* 15:43–49
- Wesley ML (1988) Use of variance techniques to measure dry air-surface exchange rates. *Boundary-Layer Meteorol* 44:13–31
- Williams CA, Scanlon TM, Albertson JD (2007) Influence of surface heterogeneity on scalar dissimilarity in the roughness sublayer. *Boundary-Layer Meteorol* 122:149–165
- Wyngaard JC, Brost RA (1984) The top-down and bottom-up diffusion of scalar in the convective boundary-layer. *J Atmos Sci* 41:102–112
- Wyngaard JC, Pennel WT, Lenschow DH, LeMone MA (1978) The temperature–humidity covariance budget in the convective boundary-layer. *J Atmos Sci* 58:35–47